

A strong-motion database from the Peru–Chile subduction zone

Maria C. Arango · Fleur O. Strasser ·
Julian J. Bommer · Ruben Boroschek ·
Diana Comte · Hernando Tavera

Received: 6 March 2010 / Accepted: 29 July 2010 / Published online: 21 August 2010
© Springer Science+Business Media B.V. 2010

Abstract Earthquake hazard along the Peru–Chile subduction zone is amongst the highest in the world. The development of a database of subduction-zone strong-motion recordings is, therefore, of great importance for ground-motion prediction in this region. Accelerograms recorded by the different networks operators in Peru and Chile have been compiled and processed in a uniform manner, and information on the source parameters of the causative earthquakes, fault-plane

geometries and local site conditions at the recording stations has been collected and reviewed to obtain high-quality metadata. The compiled database consists of 98 triaxial ground-motion recordings from 15 subduction-type events with moment magnitudes ranging from 6.3 to 8.4, recorded at 59 different sites in Peru and Chile, between 1966 and 2007. While the database presented in this study is not sufficient for the derivation of a new predictive equation for ground motions from subduction events in the Peru–Chile region, it significantly expands the global database of strong-motion data and associated metadata that can be used in the derivation of predictive equations for subduction environments. Additionally, the compiled database will allow the assessment of existing predictive models for subduction-type events in terms of their suitability for the Peru–Chile region, which directly influences seismic hazard assessment in this region.

M. C. Arango · J. J. Bommer (✉)
Department of Civil and Environmental Engineering,
Imperial College London, London SW7 2AZ, UK
e-mail: j.bommer@imperial.ac.uk

F. O. Strasser
Seismology Unit, Council for Geoscience,
Private Bag X112, Pretoria 0001, South Africa

R. Boroschek
Department of Civil Engineering,
University of Chile, Blanco Encalada 2002,
Santiago, Chile

D. Comte
Department of Geophysics, University of Chile,
Blanco Encalada 2002, Santiago, Chile

H. Tavera
Seismology Department,
Geophysical Institute of Peru, Calle Badajoz 169,
Urb Mayorazgo IV Etapa, Ate, Lima, Peru

Keywords Peru–Chile subduction zone ·
Strong-motion database · Ground-motion
processing · Site classes · Source and path
parameters

1 Introduction

The development of a strong-motion database from subduction events along the Peru–Chile

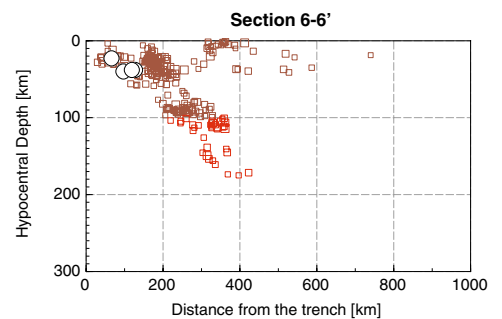
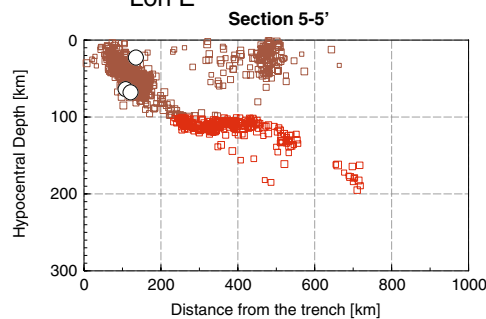
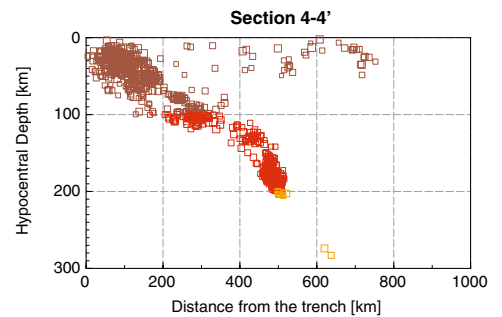
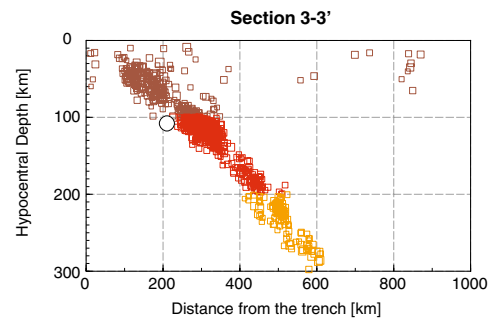
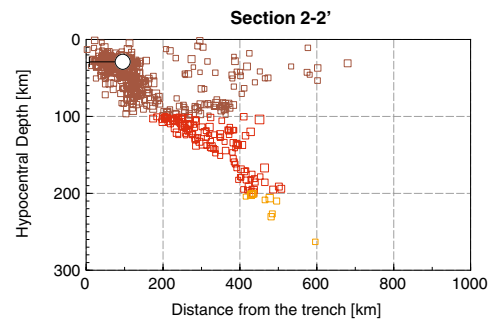
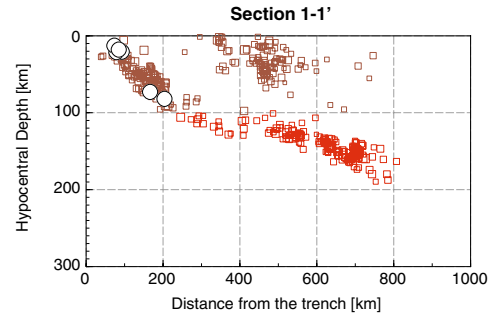
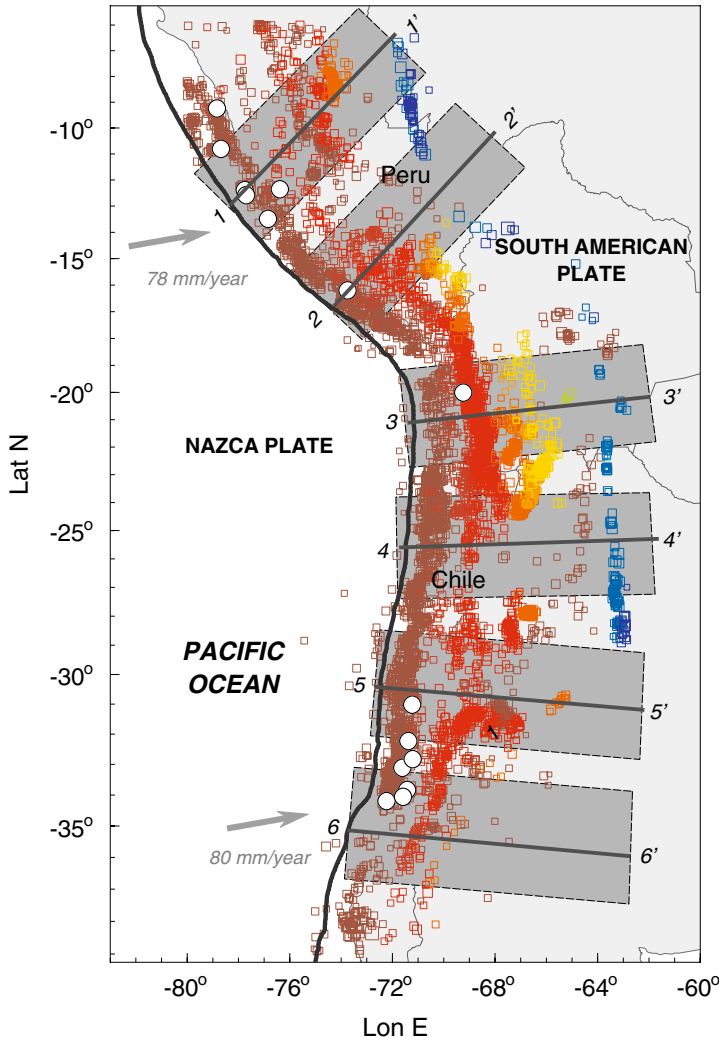
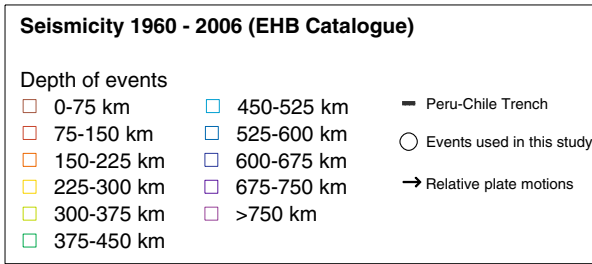
trench is an essential step for ground-motion prediction in this region as well as other subduction zones in the world where there is a significant hazard from earthquakes along the interface between the subducting and overriding plates and within the subducting slab. The tectonic setting of the Peru–Chile region is characterised by the subduction of the relatively young (~ 50 Mya) Nazca plate beneath the continental South American plate (Fig. 1), which takes place at a convergence rate of 7–9 cm/year in the N78° E direction (DeMets et al. 1990). Along the Peru–Chile subduction zone, two main types of seismicity can be identified: firstly, earthquakes occurring at the seismically coupled interface between the Nazca and South American plates (interface earthquakes) and secondly, seismicity related to the zone of extension in the interior of the descending Nazca plate (intraslab earthquakes). The Peruvian–Chilean subduction zone has frequently ruptured in great ($M \geq 8.0$) destructive earthquakes during the last centuries, many of which have been thrust-faulting events occurring along the interface between the Nazca and South American Plates, although there have also been a number of damaging intraslab events. An example of the latter is the great event (M_W 8.1) that occurred on 25 January 1939, near the city of Chillán, which killed approximately 28,000 people and is amongst the most damaging events that have occurred in the seismic history of Chile (Beck et al. 1998).

The occurrence of major subduction events along the Peruvian–Chilean subduction zone is quite frequent, with 17 events of magnitude $M_W \geq 7.5$ registered during the last 50 years. In central Chile, the historical record of earthquakes starts with an event of magnitude M 9.4 in 1575 followed by great events in 1647 (M 8.4), 1730 (M 8.2), 1822 (M 8.4) and 1906 (M 8.3; Comte et al. 1986). For instance, the great Valparaiso event of 17 August 1906 (M 8.3) caused widespread damage in central Chile and claimed thousands of lives. In recent years, the central Chile segment ruptured in a large interface earthquake on 3 March 1985 (M_W 8.0), which killed 177 people and caused extensive damage in the cities of Valparaiso and Viña del Mar. This latter event ruptured along a previously identified seismic gap

Fig. 1 Tectonic setting and distribution of seismicity along the Peru–Chile subduction zone. Seismicity corresponds to that reported in the EHB Bulletin (Engdahl et al. 1998) for the period 1960–2006 (International Seismological Centre 2009). The width and direction of the cross-sections of seismicity are indicated by the rectangles on the map

in central Chile with high probabilities of recurrence for a large earthquake (e.g., Nishenko 1985). The north-central Chile segment of subduction has also ruptured in great events in 1922 (M_W 8.7), 1943 (M_W 8.2) and 1995 (M_W 8.0). The south-central Chile segment, between 35° and 37° S, is another identified seismic gap, referred to as the Concepción–Constitución seismic gap, which has been extensively studied following the 1939 Chillán event. This segment ruptured in a great (M 8.5) earthquake in February 1835, which completely destroyed the city of Concepción. The last great earthquake in this region was the magnitude M_W 8.8 interface event that occurred on 27 February 2010, whose epicentre was located at 100 km from the city of Concepción. Preliminary reports indicated that this latter event had a death toll of more than 500 people and caused extensive damage to the cities of Concepción, Arauco and Coronel, affecting over two million people. South of this region, between 37° and 46° S, a great M_W 9.5 underthrusting event occurred on 22 May 1960, causing 1,660 deaths and leaving two million people homeless. This event, the largest instrumentally recorded in the world during the twentieth century, had an estimated rupture length of about 1,000 km (Cifuentes 1989) and also induced a tsunami that spread across the Pacific.

In the southern Peru and northern Chile segment of subduction, major interface events occurred in 1868 (southern Peru) and 1877 (northern Chile) with magnitudes estimated between 8.5 and 9.0 (Lomnitz 2004; Kausel 1986; Dorbath et al. 1990). This region had been identified as a seismic gap with a high potential of occurrence of a great earthquake (Lomnitz 2004; Kelleher 1972; Nishenko 1985; Comte and Pardo 1991; Delouis et al. 1996). The southern part of this region ruptured in a large interface event in July 1995 (M_W 8.0), which occurred south of the rupture zone of the 1877 event. Large intraslab-type events have also occurred in northern Chile in



December 1950 (M_W 8.0) and 13 June 2005 (M_W 7.8). The northern part of this seismic gap ruptured in a great interface event on 23 June 2001 (M_W 8.4), along the rupture area associated with great 1868 southern Peru event. The 2001 event had a death toll of 80 casualties and caused severe damage in the cities of Ocoña, Arequipa, Tacna and Moquegua. Along the central region of Peru, the subduction processes have caused great earthquakes in 1746 (M 8.5), 1940 (M_W 8.1), 1942 (M_W 8.0), 1966 (M_W 8.1), 1970 (M_W 7.8), 1974 (M_W 8.1), 1996 (M_W 7.7) and 2007 (M_W 8.0), causing thousands of deaths. The Central Peru segment of the subduction zone, between the rupture areas of the 1974 (M_W 8.1) Lima event and the 1996 (M_W 7.7) Nazca event (Tavera and Bernal 2005), had also been identified as another seismic gap. This gap last ruptured in a M_W 8.0 event on 17 August 2007 in the Pisco region of Central Peru, causing 595 deaths and extensive damage in the cities of Pisco, Chincha and Cañete (Tavera et al. 2008).

In view of the threat that both interface and intraslab-type events pose to the Peru–Chile region, the compilation of a strong-motion database of subduction events that can be used as the basis of future ground-motion prediction studies is of prime relevance. In Chile, the first strong-motion instruments were deployed in the 1970s by the Civil Engineering Department of the University of Chile (RENADIC network), which recorded the 3 March 1985 (M_W 8.0) Valparaiso earthquake and associated aftershocks amongst other events. Presently, the RENADIC network consists of 20 analogue and 15 digital stations installed in Northern and Central Chile. A second network (DGF-DIC) was deployed by the Departments of Geophysics and Civil Engineering of the University of Chile and the Swiss Seismological Service as a part of a project to study the northern Chile seismic gap and has been in operation since 2001. The DGF-DIC network consists of 11 digital instruments installed in Northern Chile, from Arica to Antofagasta. These two networks have recorded several large events, amongst others those on 13 June 2005 (M_W 7.8) and 23 June 2001 (M_W 8.4). The Geophysical Institute of Peru (IGP) deployed the first strong-motion instruments in Lima, which recorded the 1966, 1970,

1971 and 1974 Peruvian events. Currently, strong-motion networks in Peru are operated by IGP, the Japan–Peru Centre for Seismic Research and Disaster Mitigation (CISMID), the South American Regional Seismological Centre CERESIS, the Catholic University of Peru (PUCP), and the Peruvian state water company (SEDAPAL). Recent significant events recorded by these networks include the 23 June 2001 (M_W 8.4) and 15 August 2007 (M_W 8.0) Pisco event.

This paper presents the work performed in order to develop a database of strong-motion records from events along the Peru–Chile subduction zone and associated information (metadata). The strong-motion data recorded by the different networks operators in Peru and Chile have been compiled and processed in a uniform manner, and information on the source parameters of the causative earthquakes, fault-plane geometries and local site conditions at the recording stations has been collected and reviewed. Earthquake parameters from different reporting agencies and published studies were examined to define reliable source parameters, fault-plane geometries and distance metrics. Additionally, geological and geotechnical information at the recording sites were collected from different sources, and sites were classified according to various schemes.

2 Database description

The compiled database consists of 98 triaxial ground-motion recordings from 15 subduction-type events with moment magnitudes ranging from 6.3 to 8.4, recorded at 55 different sites in Peru and Chile, between 1966 and 2007. These accelerograms have been made available by local networks in Chile and Peru including the National Accelerographic Network of Chile (RENADIC, 23 records), the DGF-DIC network jointly operated by the Departments of Geophysics and Civil Engineering of the University of Chile (seven records), the IGP (eight records) and the CISMID (12 records). Additionally, strong-motion records from the 1985 Valparaiso (Chile) sequence and from the 1966, 1970, 1971 and 1974 Peruvian events available at the COSMOS Virtual Data Centre (<http://db.cosmos-eq.org>) were also in-

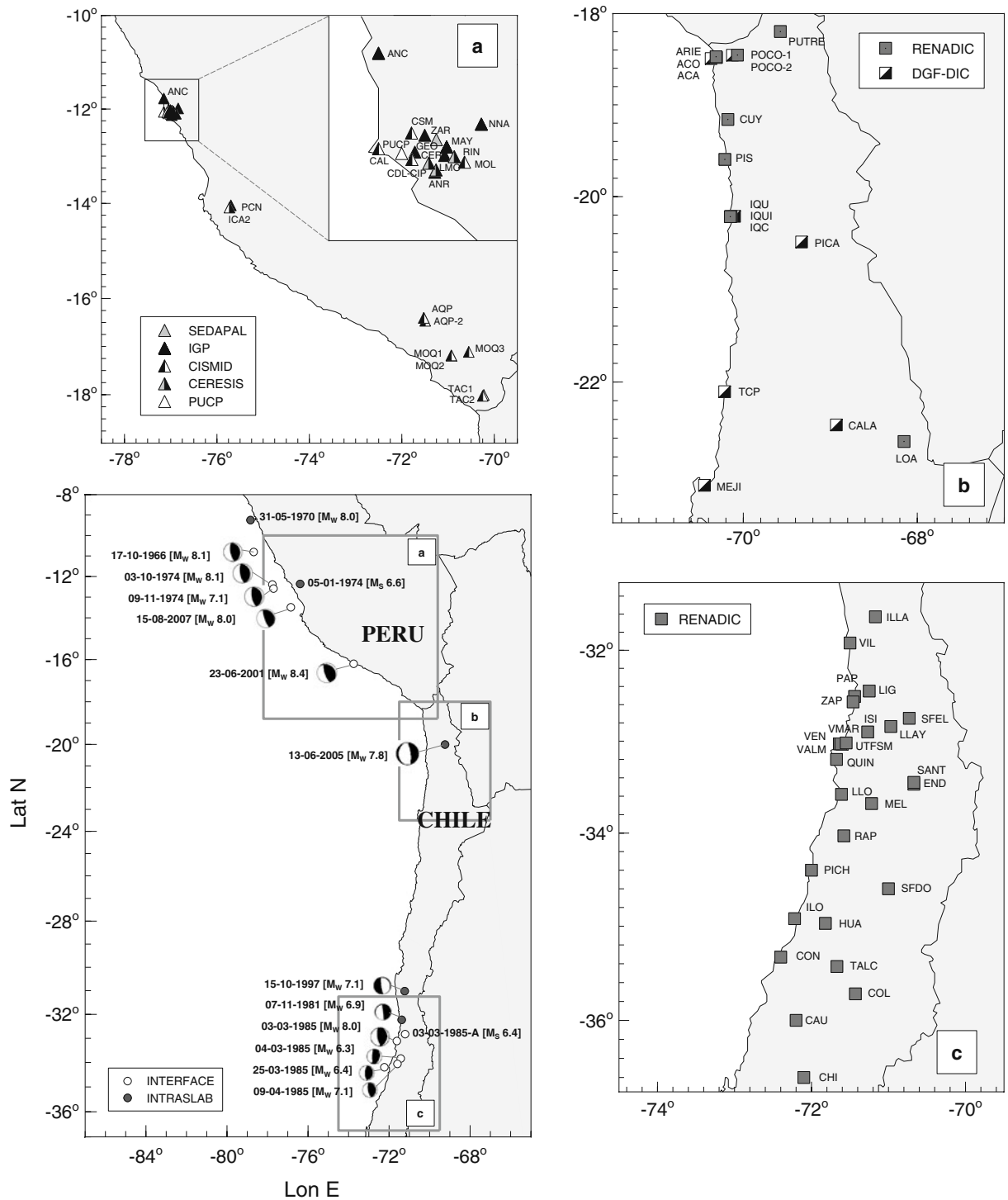


Fig. 2 Location of the strong-motion stations used in this study. The panels show the stations located in **a** Central and Southern Peru; **b** Northern Chile and **c** Central Chile. The

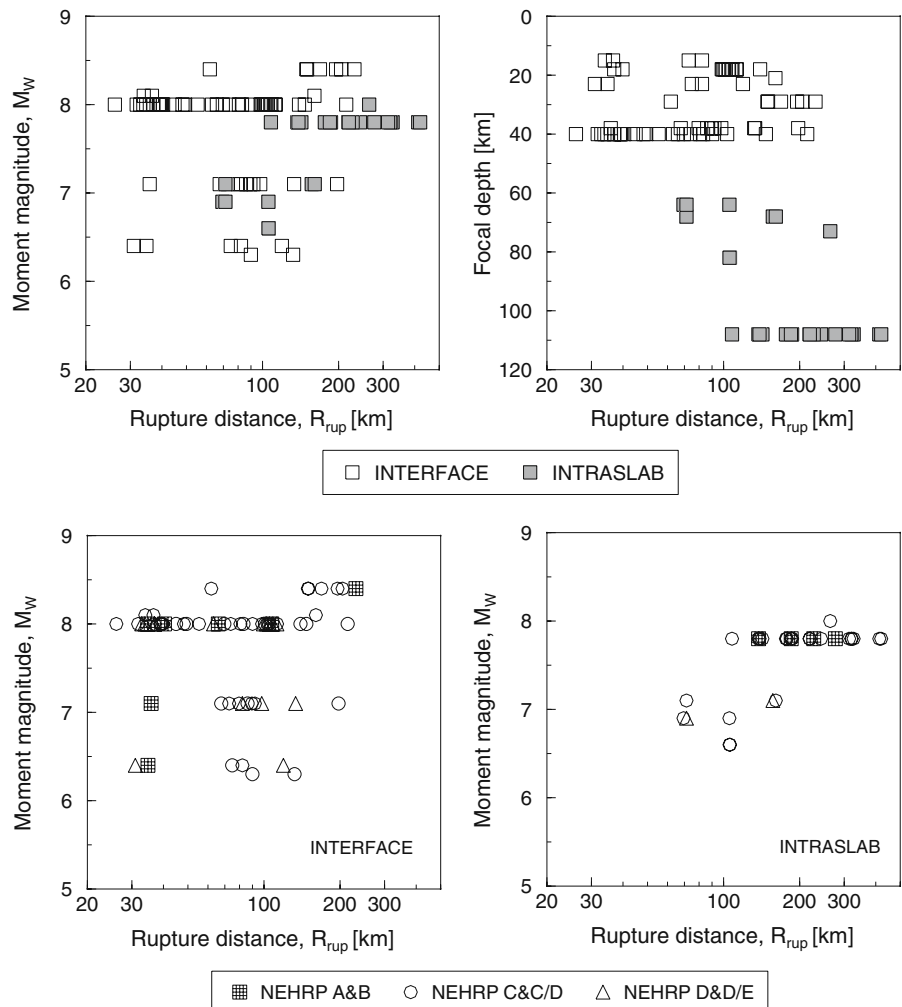
locations and focal mechanisms of the events contributing data to this study are also shown

cluded in this database (48 records). The location of the strong-motion stations operating along the Peru–Chile subduction zone, from which recordings are presented in this study, is shown in Fig. 2. The majority of the data from these agencies have been released in unprocessed format; however, in a few cases, strong-motion records to which some level of processing has already been applied were also included. All strong-motion data included in this database are from either free-field stations or instruments at the base of structures, at a total of 59 sites. In the context of this study, free-field recordings are defined as those obtained at stations in small shelters, isolated from any building influence. The other recordings are obtained from instruments at the basement of structures up to

three storeys in height, although five recordings obtained at stations located at the basement of structures with more than three storeys were included in this database.

Figure 3 displays the distribution of the data in terms of magnitude, distance, focal depth, event type and National Earthquake Hazards Reduction Program (NEHRP) site class. The methodology used in the determination of the seismological parameters, computation of distance metrics and assignment of sites is discussed in the following sections of this paper. Overall, all strong-motion data available are from moderate-to-large events ($6.3 \leq M_W \leq 8.4$) recorded at distances of about 25–420 km from the fault plane. Approximately half of the entire dataset was recorded at short dis-

Fig. 3 Distribution of the dataset in terms of magnitude, distance, focal depth, event type and NEHRP site class



tances ($R_{\text{rup}} \leq 100$ km), and consequently, a significant number of the ground motions are of large amplitudes; the level of peak ground acceleration (PGA) recorded during these events varies within a range of approximately 20–700 cm/s^2 . Similarly, most of the data included in the dataset come from events with magnitudes $M_W 8 \pm 0.3$ and $M_W 7 \pm 0.2$. The distribution of focal depth with respect to rupture distance for recordings from both interface and intraslab-type events is shown in the upper right panel of Fig. 3. The majority of the data from interface events was recorded at distances ranging from about 30 to 200 km, while the intraslab dataset includes ground motions recorded at distances R_{rup} greater than 100 km. The lower panels of Fig. 3 show the distribution of the data for interface and intraslab events by NEHRP site class. As seen from this figure, most of the strong-motion records available are from sites classified as NEHRP class C, C/D and D. Only one record from a NEHRP class D/E site is available and no data was recorded at very soft sites (NEHRP class E).

A greater emphasis has been placed on compiling and reviewing the available metadata, which entailed an evaluation of the earthquake-related parameters (i.e., magnitude, location and fault mechanism), classification of subduction events by type (i.e., interface or intraslab), computation of source-to-site distance metrics and characterisation of site conditions at recording stations using different parameters (i.e., surface geology descriptors, shear-wave velocity profiles, natural site period and normalised response spectral shapes). Site classes were assigned to the stations in Peru and Chile following various classification schemes used in ground-motion prediction equations for subduction-zone environments, such as the NEHRP classification used by Atkinson and Boore (2003, 2008), the New Zealand (NZ) site classification scheme used by McVerry et al. (2006) and the Japanese (JP) scheme used by Zhao et al. (2006b).

2.1 Earthquake-related parameters

The earthquake-related information was collected from various reporting agencies and publications and ranked by preferred importance order. The

epicentral locations and depths of the events used in this study were selected as follows: special studies of mainshock and aftershock sequences with accurate relocations, determinations published in the Centennial catalogue (Engdahl and Villaseñor 2002) and locations and depths determined by the International Seismological Centre (ISC). For the more recent events not included in the ISC catalogue, the location estimated by the National Earthquake Information Center (NEIC) was adopted. Regional determinations reported by local agencies (e.g., Department of Geophysics, University of Chile; IGP) were also used in this study when appropriate. The moment magnitude (M_W) estimates and focal mechanism solutions for the earthquakes whose data are used in this study were obtained from the Harvard Centroid Moment Tensor database (CMT) when available, which was generally the case for the large earthquakes included herein with magnitude greater than 5.0 which occurred after 1976. For all pre-1976 events, moment magnitudes and focal mechanism solutions were collected from individual studies (e.g., Hartzell and Langer 1993; Pacheco and Sykes 2002; Abe 1972). Other instrumental measures of magnitude were collected from the online-catalogues of the different reporting agencies (i.e., ISC and NEIC) and were also included in the metadata. Surface-wave magnitude (M_S) and body-wave magnitude (m_b) estimates of the Peruvian–Chilean earthquakes determined by the ISC were collected; however, in cases where ISC magnitude determinations were not available, those estimated by NEIC were used instead. No estimates of moment magnitude (M_W) were available for the 5 January 1974 (M_S 6.6) event and the 3 March 1985 (M_S 6.4) aftershock. It was, therefore, assumed that M_S estimates for these events were equivalent to moment magnitude estimates (M_W). This approximation was validated by plotting moment magnitude values against the different magnitude scales for the events with M_W , M_S and m_b data reported. The characteristics of the events contributing data to the present study are listed in Table 1; their locations and focal mechanisms are shown in Fig. 2.

Additionally, the earthquake events were classified in terms of the physical processes with which they were associated (i.e., interface or intraslab

Table 1 Summary of the earthquakes recorded in Peru and Chile, whose data are used for this study. M_W estimates were obtained from Harvard CMT catalogue, except for those events not included in there, for which M_S estimates have been listed instead (values followed by asterisk). The source of the fault geometry used to compute the rupture distance (R_{rup}) is also listed along with the number of records available from each event and the distance and PGA range. Other parameters listed include the hypocentral location, the style-of-faulting and dimensions of the fault rupture

EQ ID	Event date and time [UTC]	Epicentre ^a		Depth M_W^b [km]	S-of-F ^c	Type	Fault geometry ref ^d	Fault orientation ^e		Fault depth and length ^f		PGA range [cm/s ²]	Data availability			
		Lat [°S]	Lon [°W]					Strike [°]	Dip [°]	H _{top} [km]	H _{hinge/RL} [km]			H _{bottom} [km]	# records	R_{rup} range [km]
1	17/10/1966 [21:41:56]	10.807	78.684	20.7	8.1	R	Interface Abe (1972)	335	12	4.5	35	80	1	168	396	COSMOS ^g
2	31/05/1970 [20:23:32]	9.248	78.840	73.0	8.0	N	Intraslab Abe (1972)	340	53	36	90	130	1	265	129	COSMOS ^g
3	05/01/1974 [08:33:51]	12.360	76.390	82.0	6.6*	N	Intraslab From scaling relations	315	35*	76	87	23	2	105–107	88–169	COSMOS ^g
4	03/10/1974 [14:21:29]	12.390	77.760	15.0	8.1	R	Interface Hartzell and Langer (1993)	350	11/30	2.4	24/52	250	2	34–37	196–245	COSMOS ^g
5	09/11/1974 [12:59:52]	12.587	77.705	15.0	7.1	R	Interface Hartzell and Langer (1993)	350	11	4	21	60	2	73–82	49–118	COSMOS ^g
6	07/11/1981 [03:29:52]	32.232	71.379	63.9	6.9	N	Intraslab From scaling relations	345	86	52	76	34	3	54–93	285–571	RENADIC ^h (upon request)
7	03/03/1985 [22:47:09]	33.115	71.616	40.0	8.0	R	Interface Mendoza et al. (1994)	5	15/30	6.4	26/71	255	25	26–215	24–707	COSMOS ^g
8	03/03/1985 [23:38:30]	32.829	71.211	22.8	6.4*	–	Interface From scaling relations	11	26	18	28	19	3	31–83	32–187	COSMOS ^g
9	04/03/1985 [15:01:08]	33.837	71.426	38.0	6.3	R	Interface Choy and Dewey (1988)	21	28	35	41	12	2	89–132	57–230	RENADIC ^h (upon request)
10	25/03/1985 [05:14:33]	34.198	72.233	23.0	6.4	R	Interface Choy and Dewey (1988)	10	20	21	25	13	2	75–119	31–101	RENADIC ^h (upon request)

11	09/04/1985 [01:57:01]	34.060	71.589	38.0	7.1	R	Interface	Choy and Dewey (1988)	0	21	33	43	26	9	36–197	21–158	COSMOS ^e
12	15/10/1997 [01:03:35]	31.020	71.230	68.0	7.1	N	Intraslab	From scaling relations	173	80	54	82	43	3	72–161	50–347	RENADIC ^b (upon request)
13	23/06/2001 [20:33:15]	16.200	73.750	29.0	8.4	R	Interface	Pritchard et al. (2007)	310	11/25	7.5	25/70	310	7	62–231	31–330	RENADIC ^b (upon request)
14	13/06/2005 [22:44:32]	20.010	69.240	108.0	7.8	N	Intraslab	Delouis and Legrand (2007)	175	15/35	105.4	115/132	110	23	108–420	18–708	CISMID ⁱ RENADIC ^b (upon request)
15	15/08/2007 [23:40:59]	13.490	76.850	18.0	8.0	R	Interface	Ji and Zeng (2007)	323	27	3.5	52	190	13	37–139	19–488	CISMID ⁱ IGPI (upon request)

R reverse, *N* normal, H_{top} depth to top, H_{bottom} depth to bottom, *RL* rupture length as measured along the strike

^aEpicentre locations and depths from the following references: Engdahl and Villaseñor (2002) [Events 1, 2, 6, 8], Langer and Spence (1995) [Events 3, 4, 5], Choy and Dewey (1988) [Events 7, 9, 10, 11], [3] Pardo et al. (2002a) [Event 12], Tavera et al. (2002) [Event 13], Delouis and Legrand (2007) [Event 14], Tavera et al. (2008) [Event 15]

^b M_w estimates are taken from the CMT catalogue. For events earlier than 1976, the values reported come from the following references: Abe (1972) and Stauder (1975) [Events 1, 2], Langer and Spence (1995) [Event 3], Hartzell and Langer (1993) [Events 4, 5]

^cStyle-of-Faulting: R, N following the Wells and Coppersmith (1994) definitions

^dFault plane dimensions of events of unknown geometry have been defined using the Strasser et al. (2010) scaling relations for subduction-zone events

^eFault plane orientation from the selected fault model. Events for which a finite source model is not available, the strike and dip have been selected from the two sets of angles reported in the Harvard CMT catalogue (see text for explanation). Two dip values are reported for hinged fault models

^fFor multi-segment models, the depth to the hinge in the fault is also reported (H_{hinge})

^gStrong-motion records downloadable at <http://db.cosmos-eq.org>

^hInterested readers shall contact the 4th author regarding strong-motion records availability (borosch@cec.u Chile.cl)

ⁱStrong-motion records downloadable at <http://www.cismid-umi.org/>

^jInterested readers shall contact the 6th author regarding strong-motion records availability (hernando.tavera@igp.gob.pe)

activity). The earthquake classification was made on the basis of focal mechanism, epicentral location, depth and relative position with respect to the trench axis. The dominant mechanism of interface-type earthquakes corresponds to thrust faulting on shallow-dipping planes that are oriented approximately parallel to the trench axis. At depths greater than the coupled plate interface, the stress regime changes from compressional to tensional and thus normal faulting prevails. These normal mechanism events are associated with intraslab activity occurring within the subducted Nazca slab, at some distance down-dip from the seismically coupled interface. At intermediate depths, two types of intraslab earthquakes have been identified in this region (e.g., Lemoine et al. 2002): slab-push and slab-pull, which are associated with down-plate compression and extension, respectively. Along the Peru–Chile subduction zone, the occurrence of slab-pull events is relatively common in comparison with slab-push events, although some slab-push events have occurred in North-Central Chile (the 15 October 1997 Punitaqui earthquake) and Central Peru (the 5 and 29 April 1991 earthquakes).

The differentiation between interface and intraslab events was performed using the definitions of style-of-faulting of Wells and Coppersmith (1994) and the event depth and location with respect to the trench axis. As seen in Table 1, the interface events in this catalogue have a reverse mechanism and are limited to a maximum depth of 40 km, which is consistent with the maximum depth extent of the seismically coupled zone found along different segments of the Peru–Chile subduction zone (e.g., Comte et al. 1994; Comte and Suárez 1995; Tichelaar and Ruff 1991). On the other hand, intraslab-type events in Table 1 have a normal mechanism and occur within the Nazca slab at depths from about 60 to 110 km. The location of these events in 3D space combined with information regarding their focal mechanism (Fig. 1 and lower left panel of Fig. 2) allows a fairly unambiguous classification between interface and intraslab events, particularly since the geometry of the subducting Nazca slab has been extensively documented. The geometry of the subducting Nazca plate is characterised by variations in the dip angle along the strike of the trench (Barazangi

and Isacks 1976; Jordan et al. 1983; Cahill and Isacks 1992). Between latitude 8° and 45° S, the subducting Nazca plate is divided into four segments: northern and central Peru, from 8° to 15° S, where the subducted Nazca plate has a shallow dip of about 10°; southern Peru and northern Chile, from 15° to 27° S, where the Nazca Plate descends with a dip of 25° to 30°. In Central Chile, from 27° to 33° S, the slab is again relatively flat, with a shallow dip angle of about 10°, and in southern Chile, from 33° to 45° S, the dip of the subducted slab increases to 30°.

The depth extent of the seismically coupled plate interface along the Peru–Chile subduction zone is similarly well-documented. It has been estimated from the maximum depth of shallow-dipping reverse events (e.g., Tichelaar and Ruff 1991; Suárez and Comte 1993; Comte et al. 1994; Comte and Suárez 1995) and from the depth transition from compressional to extensional stress regime (e.g., Comte and Suárez 1995; Pardo et al. 2002b). Based on the maximum depth of large ($M_w > 6$) under-thrusting events located teleseismically, Tichelaar and Ruff (1991) suggested that the maximum depth of the seismically coupled zone between plates along Chile extends down to 48–53 km and that there is a change in the maximum depth north of latitude 28° S, where the coupled zone extends to depths of 36–41 km. In contrast, studies using both locally and teleseismically recorded data in Northern Chile (Comte et al. 1994; Comte and Suárez 1995) suggest that the coupling zone, as defined by the maximum depth observed for shallow-dipping reverse events, extends consistently to about 40 ± 10 km and no variations along the strike of the trench are appreciable. The maximum depth of the coupling zone may, however, extend up to 60 ± 10 km, if the depth transition from compressional to tensional stress regime observed along the upper part of the subducting slab is considered (Comte and Suárez 1995). This transition of stress field along the Northern Chile segment occurs at depths greater than the maximum depth at which shallow-dipping reverse events are observed (~ 40 km). Along the Central Chile segment of the subduction zone, the maximum depth of the plate interface has also been estimated to be about 60 km (Pardo et al. 2002a), which

is in agreement with the aforementioned studies along different segments of the Chilean subduction zone.

2.2 Station information and assignment of site conditions

The coordinates of the stations used in this study, type of instrument and instrument housing are listed in Tables 2 and 3 and their geographical distribution is shown in Fig. 2. For the stations in Central Chile that recorded the 1985 Valparaíso earthquake sequence, some of which are no longer in operation, the station coordinates listed correspond to those reported by Campbell et al. (1989, 1990), which were validated against satellite imagery (i.e., Google Earth) to ensure accuracy. Information on the type and location of instrument (i.e., type of building) was also obtained from these references, from the accelerogram headings and from the websites of the network operators (IGP, CISMID, RENADIC and DGF-DIC). Information on the majority of the Peruvian stations included herein has already been presented in Tavera et al. (2008).

Tables 2 and 3 also summarise all geological and geotechnical information collected for the sites contributing data to this study. Site conditions assigned to the stations in Central Chile were based on information collected from a number of references including descriptions of the surface geology (EERI 1986; Çelebi 1987, 1988; Campbell et al. 1989, 1990; Midorikawa et al. 1991; Midorikawa 1992), the site categories following the Chilean seismic design code assigned by Riddell (1995) and NEHRP site classes assigned by Atkinson and Boore (2003) to the Chilean sites whose data were included in the regression database for subduction-zone events. Shear-wave velocity (V_S) profiles obtained by Araneda and Saragoni (1994), Midorikawa et al. (1991) and Midorikawa (1992) in addition to the natural period of the Chilean sites determined by Luppichini (2004) using the records of the 1985 Valparaíso earthquake, were also used. Site conditions at the strong-motion stations in Northern Chile are still under investigation and geological and geotechnical information for a number of these stations

has not yet been made available to the wider engineering community. It is believed, however, that recording sites in Northern Chile can be classified as NEHRP class C, with an average shear-wave velocity over the top 30 m, V_{S30} , between 400 and 600 m/s (Boroschek and Comte 2006). Therefore, site conditions assigned to these sites were only based on information from descriptions of the local geology (SNGM 1982), V_S profiles obtained from spectral analysis of surface waves (SASW) measurements at the stations in Arica and Poconchile (Cortez-Flores 2004), and natural site periods estimated by site response analysis for the Arica and Poconchile stations (Cortez-Flores 2004).

Site conditions assigned to the stations in Central and Southern Peru were based on descriptions of the surface geology (EERI 2007; Bernal and Tavera 2007a, b) and the site category (i.e., rock, soil or firm ground) assigned by Rodríguez-Marek et al. (2007). Shear-wave velocity (V_S) profiles obtained from SASW measurements at the stations in Ica (Rosenblad and Bay 2008) and the stations in Moquegua and Tacna (Cortez-Flores 2004), as well as the V_S profiles estimate by Bernal and Tavera (2007a, b) using an infinite flat-layered half-space model were also used. Additionally, the natural site period as interpreted from the microzonation map of Lima (Aguilar Bardales and Alva Hurtado 2007) and that estimated by site response analysis for the Moquegua and Tacna sites (Cortez-Flores 2004) were included. Information on the site conditions of the majority of the Peruvian stations included herein has been also been reported in Tavera et al. (2008).

Besides the site information collected, the spectral shapes of the records were considered by normalising the response spectra by their PGA value (for all records) and by dividing the spectra recorded at soil stations by the spectrum obtained on rock, for stations sufficiently close to one another. The natural period for each site computed from earthquake records, $T_{0,REC}$, was also estimated and used as a guide for the assignation of site classes, following the empirical site classification approach (JP) adopted by Zhao et al. (2006a) which defines the site period as that corresponding to the highest H/V response spectral

Table 2 Summary of characteristics of Chilean strong-motion stations used in this study

Instrument & station information			Geological & geotechnical information										Site classes assigned				
Code ^a	Name	Lat [°S]	Lon [°W]	IT ^b	IL ^c	Surface geology ^d	SC ^e _{AB}	SC ^f _{CF}	SC ^g _R	V ^h _{S30}	T ⁱ _{0,LUP}	T ^j _{0,CF}	T ^k _{0,REC}	NH ^l	NZ ^m	JP ⁿ	CO ^o
ACA [REN]	Arica-Casa	18.482	70.308	S	B1	Marine and continental sediments on rock ^[1] ;	-	C ₂	-	432 ^[1]	-	T _{S1} = 0.15 T _{S2} = 0.19	0.13–0.34	C	C	II	II
ACO [REN]	Arica Costanera	18.474	70.313	S	B	Marine and continental sediments on rock ^[1] ;	-	C ₂	-	389 ^[1]	-	T _{S1} = 0.32 T _{S2} = 0.36	0.33–0.39	C	C	II	II
ARIE [D-D]	Arica Escuela	18.494	70.312	E	B1	Volcanic rock ^[1] ;	-	B	-	1132 ^[1]	-	T _{S1} = 0.11	0.38	B	B	I	I
CALA [D-D]	Calama Hospital	22.459	68.930	E	B	Sediments ^[2] ;	-	-	-	-	-	-	~0.10	C	C	II	II
CAU [REN]	Cauquenes	35.97	72.32	S	B2	Deep sediments ^[3] ;	D	-	II	648 ^[2]	0.45	-	0.40–0.62	C/D	C	III	II
CHIL [REN]	Chillán-Viejo	36.60	72.10	S	B2	Dense gravel ^[6] ;	-	-	II	568 ^[2]	0.77	-	0.35–0.56	C/D	C	III	II
CONS [REN]	Constitución	35.33	72.41	S	B2	Soft alluvium ^[5] ;	D	-	III	595 ^[2]	0.83	-	~0.74	C/D	D	III	III
CUY [REN]	Cuya	19.160	70.177	S	U	Dense gravel ^[6] ;	-	-	-	-	-	-	-	C	C	II	II
END [REN]	Santiago Endesa	33.45	70.65	P	B6	Granite ^[4,7] ;	-	-	-	513 ^[3]	0.33	-	0.70–0.81	C	C	III	II
						Paleozoic intrusive ^[5] ;											
						Medium density sand ^[6]											
						Sedimentary rock and marine sediments ^[1]											
						Firm gravel ^[4] ;											
						Alluvium ^[5] ;											
						Shallow fill on dense gravel ^[8]											

HUA [REN]	Hualañe	34.97	71.82	S	B1	Alluvium ^[4,7] ; Dense gravel ^[6]	B	-	II	527 ^[2]	0.38	-	~0.36	C/D	C	II	II
ILLA [REN]	Illapel	31.63	71.17	S	B1	Alluvium ^[4,7] ; Dense gravel ^[6]	E	-	II	613 ^[2]	0.25	-	0.16–0.22	C	C	II	II
ILO [REN]	Iloca	34.93	72.18	S	B1	Alluvium ^[4,5,7] ; Sand ^[6]	D	-	II	555 ^[2]	0.33	-	0.22–0.43	C/D	C	II	II
IQU [REN]	Iquique-Idiem	20.215	70.140	S	B	Sediments ^[2]	-	-	-	-	-	-	~0.50	C	B	III	II
IQU [REN]	Iquique-Inp	20.217	70.149	S	B	Sediments ^[2]	-	-	-	-	-	-	~0.53	C	C	III	II
IQU [D-D]	Iquique Hospital	20.214	70.138	E	B	Rock ^[2] ; Rock ^[3]	-	-	-	-	-	-	~0.40	B	C	I	I
ISID [REN]	San Isidro	32.90	71.27	S	U	Alluvium ^[1]	D	-	-	789 ^[2]	0.33	-	0.37	C	C	II	II
LIG [REN]	La Ligua	32.45	71.25	S	B1	Alluvium ^[4,7] ; Dense gravel ^[6]	D	-	II	620 ^[2]	0.29	-	-	C	C	II	II
LLAY [REN]	Llay Llay	32.84	70.97	S	B1	Soft alluvium ^[4,7] ; Gravel and soft lime ^[6]	E	-	II	610 ^[2]	0.67	-	~1.0	D	D	III	III
LLO [REN]	Llolleo	33.58	71.61	S	B1	Sandstone and volcanic rock ^[4,7] ; Dense sand ^[6]	-	-	II	305 ^[2]	0.53	-	0.42–0.52	C/D	C	III	II
LOA [REN]	El Loa	22.636	68.152	S	U	Volcanic rock ^[1]	-	-	-	-	-	-	~0.12	B	C	I	I
MEJI [D-D]	Mejillones - Hospital	23.103	70.446	E	B	Sediments ^[2] ; very deep sands ^[3]	-	-	-	-	-	-	0.33–0.85	C	D	III	III
MELP [REN]	Melipilla	33.68	71.22	S	B1	Alluvium ^[4] ; Dense sand ^[6] ; Granite ^[7]	C	-	II	724 ^[2]	0.30	-	0.20–0.35	C	C	II	II
PAP [REN]	Papudo	32.51	71.45	S	B1	Granite ^[4,7] ; Weathered rock ^[6]	B	-	I	517 ^[2]	0.34	-	0.26–0.36	C/D	C	II	II
PICA [D-D]	Pica - Hospital	20.492	69.330	E	B	Sediments ^[2]	-	-	-	-	-	-	~0.35	C	C	II	II

Table 2 (continued)

Instrument & station information			Geological & geotechnical information										Site classes assigned				
Code ^a	Name	Lat [°S]	Lon [°W]	IT ^b	IL ^c	Surface geology ^d	SC _{AB} ^e	SC _{CF} ^f	SC _R ^g	V ₃₃₀ ^h	T _{0,LUP} ⁱ	T _{0,CF} ^j	T _{0,REC} ^k	NH ^l	NZ ^m	JP ⁿ	CO ^o
PICH [REN]	Pichilemu	34.38	72.02	S	B1	Slates, sandstone, limestone ^[4,7] , Rock ^[6]	B	-	I	623 ^[2]	0.33	-	~0.23	C	B	II	I
PIS [REN]	Pisagua	19.595	70.212	S	U	Shallow fill on weathered rock ^[3]	-	-	-	-	-	-	0.10–0.33	C	B	II	I
POCO1 [REN]	Poconchile 1	18.456	70.067	S	B	Marine and continental sediments on rock ^[1]	-	C ₂	-	511 ^[1]	-	T _{S1} = 0.24 T _{S2} = 0.22	0.21–0.57	C	C	II	II
POCO2 [D-D]	Poconchile 2	18.457	70.107	E	B	Marine and continental sediments on rock ^[1]	-	C ₂	-	-	-	T _{S1} = 0.24 T _{S2} = 0.22	0.21	C	C	II	II
PU [REN]	Putre	18.197	69.574	S	U	Weathered rock ^[3] on rock ^[1]	-	-	-	-	-	-	0.38–0.56	C	B	III	II
QUIN [REN]	Quintay	33.20	71.68	S	S	Paleozoic intrusives ^[5] , Rock ^[6]	-	-	I	595 ^[2]	0.50	-	0.48–0.66	C	B	II	I
RAP [REN]	Rapel	34.03	71.58	R	T	Sediments ^[4,7] ; Paleozoic intrusives ^[5] , Rock ^[6]	B	-	I	3010 ^[2]	0.40	-	0.10–0.29	A	A	I	I
SANT [REN]	Santiago	33.47	70.67	S	B3	Firm gravel ^[4] ; Alluvium ^[5]	-	-	-	-	0.65	-	0.66–0.91	C	C	III	II
SFDO [REN]	San Fernando	34.60	71.00	S	B1	Alluvium ^[4,7] ; Dense gravel ^[6]	D	-	II	543 ^[2]	0.36	-	0.22–0.46	C	C	II	II
SFEL [REN]	San Felipe	32.75	70.73	S	B1	Alluvium ^[4,7] ; Dense gravel ^[6]	D	-	II	502 ^[2]	0.50	-	~0.12	C	C	II	II
TAL [REN]	Talca	35.43	71.67	S	B1	Alluvium ^[4,7] ; Dense gravel ^[6]	E	-	II	598 ^[2]	0.83	-	0.17	C	C	II	III
TCP [D-D]	Tocopilla	22.104	70.214	E	U	Rock ^[2]	-	-	-	-	-	-	~0.10	B	B	I	I

UTFSM [REN]	Valparaiso UTFSM	33.03	71.60	S	B1	Volcanic rock ^(4,7) ; Rock ⁽⁶⁾	B	-	I	1421 ⁽²⁾	1.00	-	0.78–0.87	A	A	I	I
VALMD [REN]	Valparaiso El Almendral	33.03	71.64	S	R	Fill ^(4,6) ; Soil ⁽⁷⁾ ; Artificial fill ⁽⁸⁾	D	-	III	360 ⁽³⁾	0.67	-	-	D	D	III	III
VENT [REN]	Ventanas	33.03	71.62	S	B6	Loose sand ⁽⁴⁾ ; Alluvium ⁽⁵⁾ ; Sand ^(6,7)	D	-	III	331 ⁽²⁾	0.67	-	0.76–1.0	D	D	III	III
VIL [REN]	Los Vilos	31.92	71.50	S	B1	Sedimentary rock ^(4,7) ; Rock ⁽⁶⁾	B	-	I	1215 ⁽²⁾	-	-	0.26	A	B	I	I
VMAR [REN]	Viña del Mar	33.02	71.55	S	B10	Alluvium and sand ⁽⁴⁾ ; Sand ⁽⁶⁾	-	-	III	273 ⁽³⁾	0.50	-	0.50–0.80	D	D	III	I
ZAP [REN]	Zapallar	32.55	71.46	S	B1	Rock ⁽⁶⁾ ; Granite ⁽⁷⁾	B	-	I	605 ⁽²⁾	0.41	-	~0.18	C	B	II	II

^aStation code, followed by the network: REN=RENADIC; D-D=DGC-DIC

^bInstrument type: E=ETNA; P=PK-130; R=RFT-250; S=SMA-1;

^cInstrument location: B=building, followed by number of storeys if known; S=shelter; T=tunnel; U=unknown

^dDescription of the surface geology, based on the following references: [1] Geologic map of Chile (SNGM 1982); [2] Alva Hurtado (2005); [3] this study; [4] Celebi (1988); [5] Campbell et al. (1990); [6] Riddell (1995); [7] EERI reconnaissance report (1986); [8] Midorikawa et al. (1991) and Midorikawa (1992)

^eNEHRP site classes assigned by Atkinson and Boore (2003, 2008)

^fSite classes assigned by Cortez-Flores (2004) following the Rodriguez-Marek et al. (2001) site classification scheme: B=Rock; C₂=Shallow stiff soil

^gSoil classes assigned by Riddell (1995) following the 1993 Chilean seismic design code provisions

^hAverage shear-wave velocity over the top 30 m, in m/s, determined from: [1] V_s profiles obtained by Cortez-Flores (2004) using SASW; [2] V_s profiles determined by Araneda and Saragoni (1994); V_s profiles obtained by Midorikawa et al. (1991) and Midorikawa (1992). For calculation purposes, when V_s data were available at depths <30 m, the V_s value of the last layer was assumed constant to 30 m depth

ⁱPredominant site period, in seconds, determined by Luppichini (2004). Values listed as reported by Ruiz and Saragoni (2005)

^jPredominant site period determined by Cortez-Flores (2004). T_{S1} was estimated as the period corresponding to the maximum ratio of response spectra at the surface over the response spectra of outcrop input motion and T_{S2} corresponds to the characteristic site period calculated from the equation T_S = 4H/V_s

^kPredominant site period calculated from acceleration by considering the H/V ratio of the response spectra, following the approach of Zhao et al. (2006a). The lower and upper boundaries of the interval reported correspond to the maximum and minimum values of the natural site period found when using multiple records from the same station. Values are only listed for those records whose vertical component is available

^lSite class according to the NEHRP (1997) provisions used in analyses

^mSite class assigned following the New Zealand site classification, which is based on surface geology, geotechnical properties, natural site period and depth to bedrock (see McVerry et al. 2006 for details)

ⁿSite class assigned following the Zhao et al. (2006b) scheme, considering the natural period of the site

^oSite class assigned to compute the design loads prescribed by the 1996 Chilean seismic code

Table 3 Information on Peruvian strong-motion stations used in this study

Code	Name	IT	Lat [°S]	Lon [°W]	Loc	Surface geology ^a	SC ^{RM}	V _{S30} [m/s]	T _{0,CIS} ^d	T _{0,REC} ^c	NH ^f	NZ ^B	JPh ^h	CO ⁱ	
ANC [IGP]	Ancon	D	11.776	77.150	U	Alluvial gravel (soil) ^[2]	S	280 ^[5]	0.2–0.3	0.30	0.10	C/D	C	II	II
ANR [CER]	Asamblea Nacional de Rectores	D	12.123	76.976	B	Alluvial gravel (soil) ^[2]	FG	205 ^[5]	0.2–0.3	0.50	0.15	D	C	II	II
CAL [CIS]	Callao	E	12.060	77.150	S	Soft soil ^[1] ; Soft clay ^[2] ; Granular fill over fine stratified soils ^[3]	S	75 ^[5]	0.5–0.6	0.53	0.52	D/E	E	IV	III
CDL-CIP [CIS]	CDL-CIP	E	12.092	77.049	S	Dense, stiff gravel deposit (Lima Conglomerate) ^[1] ; Alluvial gravel (soil) ^[2]	FG		0.1–0.2	0.82	0.30	D	C	III	II
CER [CER]	Ceresis	E	12.103	76.998	U	Alluvial gravel (soil) ^[2]	FG		0.1–0.2	0.28	0.45	D	C	III	II
CSM [CIS]	Cismid	D	12.013	77.050	B1	Dense, stiff gravel deposit (Lima Conglomerate) ^[1] ; Alluvial gravel (soil) ^[2]	FG	184 ^[5]	0.2–0.3	0.05	0.10	C	C	II	I
GEO [IGP]	Geological Institute	A	12.08	76.95	U	Coarse dense gravel				–		C	B	II	II
HUA [IGP]	Casa Huaco – Las Gardenias	A	12.13	76.98	U	Alluvial deposits				–		C	B	II	II
ICA2 [CIS]	Ica 2	A	14.089	75.732	B	Silty sand, soil ^[1]	S	312	–	0.72	0.48	D	C	III	II
LMOL [IGP]	La Molina Universidad Agraria	A	12.085	76.948	U	Alluvial deposits (soft clays and sand) ^[4]									
MAY [IGP]	Mayorazgo	D	12.055	76.944	U	Sand and silt ^[2]	S	276 ^[5]	0.2–0.3	0.22	0.20	C	C	II	I
MOL [CIS]	Molina	E	12.10	76.89	B	Shallow soil overlying dense Lima Conglomerate; Sand ^[2]	R	380 ^[5]	0.2–0.4	0.13	0.20	C	C	II	I

MOQ1 [CIS]	A	17.187	70.929	S	Alluvial deposits (sandy gravels) ^[5]	573	0.11–0.18	C	B	II	II
NNA [IGP]	D	11.987	76.389	U	Rock ^[2]	–	0.10 0.22	B	B	I	I
PCN [IGP]	D	14.042	75.699	U	Soil ^[1]	S	0.42 0.54	C/D	C	III	II
PUCP [PUCP]	D	12.074	77.080	B	Alluvial gravel (soil) ^[2]	FG	0.2–0.3	D	D	III	II
RIN [CER]	D	12.084	76.921	U	Fill consisting of sand, silt and gravel ^[2]	S	0.2–0.3	C/D	C	II	II

^aDescription of surface geology profile, based on the following references: [1] EERI (2007) [2] Bernal and Tavera (2007a, b) [3] information provided by the strong-motion network in the accelerogram heading [4] Espinosa et al. (1977) [5] Cortez-Flores (2004)

^bSite class assigned by Rodriguez-Marek et al. (2007)

^cAverage shear-wave velocity over the top 30 m. For the Ica stations, this is based on the V_s profiles obtained by Rosenblad and Bay (2008) using SASW. For the Lima stations, the value tabulated is a tentative estimate of V_{S30} based on the V_s profile inferred by Bernal and Tavera (2007a, b) using an infinite flat-layered half-space model

^dNatural site period (T_0) inferred from the microzonation map of Lima (Aguilar Bardales and Alva Hurtado 2007). Values are not available for the NNA station in Lima, nor for the Ica stations

^ePredominant period calculated from accelerogram by considering the H/V ratio of the response spectra, following the approach of Zhao et al. (2006a). The top value corresponds to the east-west component of motion, while the bottom value corresponds to the north-south component

^fSite class according to the NEHRP (1997) provisions. The number in brackets corresponds to the V_{S30} value assumed when explicitly required, following the recommendations of Atkinson and Boore (2003)

^gSite class according to the New Zealand site classification, which is based on surface geology, geotechnical properties and depth to bedrock. See McVerry et al. (2006) for details

^hSite class according to the Zhao et al. (2006b) scheme, considering V_{S30} and the natural period of the site

ⁱSite class assumed to compute the design loads prescribed by the 1977 and 2003 Peruvian seismic codes

ratio. Tables 2 and 3 also list the site classes assigned to the different stations following several classification schemes: the NEHRP site classification, which is based on the average shear-wave velocity over the top 30 m; the New Zealand classification scheme used by McVerry et al. (2006), which classifies sites on the basis of the surface geology, geotechnical properties, site period and depth to bedrock; and the JP scheme used by Zhao et al. (2006b), which uses the predominant site period from H/V response spectral ratios.

Due to the inherent limitations of some of the site data collected, the same level of priority was not given to all the various pieces of information in the assignment of site classes. For instance, only V_S profiles determined from measurements of shear-wave velocity conducted in the field have been used for the direct assignment of site classes, and profiles reported from inversions (e.g., Bernal and Tavera 2007a, b) have only been used to distinguish between shallow and deep soil sites since in several instances these profiles have been found to be biased towards low values, leading to site classifications that are inconsistent with other geological and geotechnical descriptions. Similarly, the V_{S30} values listed in Table 2, calculated from the V_S profiles estimated by Araneda and Saragoni (1994) at a number of sites in central Chile (i.e., LLAY, MEL, ISI), were found to be biased towards high values. As no information as to the manner in which the V_S values published in Araneda and Saragoni (1994) were obtained (i.e., in situ measurements or numerical modelling), these V_S profiles have only been used to identify different soil depths. In addition, the natural period ($T_{0,CIS}$) derived using ambient noise measurements mapped in the microzonation map of Lima (Aguilar Bardales and Alva Hurtado 2007), was generally the preferred input for assigning the JP site classes to the Peruvian sites as the predominant period calculated directly from the records ($T_{0,REC}$) could be biased due to non-linearity effects. In some instances, however, it was found that mapped period was inconsistent with other site descriptors, possibly due to limitations of the mapping resolution. For the stations in Chile, natural periods estimated by site response analysis (Cortez-Flores 2004) were the preferred input.

Most of the stations in Central Chile are situated on dense alluvial gravel and sand classified as NEHRP class C, C/D and D. There are no stations situated on soft soil (NEHRP E); however, the VMAR and V-ALM stations are on deep sand and artificial fill, respectively, and, therefore, exhibit features consistent with soils of medium density. These sites are classified as NEHRP D in view of the large values of the V_{S30} reported. Only three stations are located on hard rock and rock (NEHRP class A and B), and three sites are on soft/weathered rock classified as NEHRP class C: the RAP, VIL and UTFSM stations are located on rock (NEHRP site class B) and ZAP, QUI, PIC sites are on soft/weathered rock (NEHRP site class C). Stations in Northern Chile are situated on volcanic rock and shallow fill on weathered rock, classified as NEHRP B and C, respectively. The most recent material in this region consists of Quaternary alluvial and fluvial deposits and many of the stations are located on such material. These sites are, therefore, classified as NEHRP C by virtue of the V_{S30} values estimated for some of those sites (ACA, ACO, POCO1, POCO2) as well as the shape of the normalised spectra (IQU, MEJI, PICA, CUY). The majority of the stations in Peru used in this study are situated on alluvial gravel, sand and silt and have been classified as NEHRP class C and D and only one station (NNA) is situated on rock classified as NEHRP class B. Conversely, the station CAL is located close to the coast in an area of reclaimed land over soft soil, and has been classified as NEHRP class D/E. Another station located on reclaimed land is RIN, which is located on loose granular fill composed of gravel, silt and fine sand.

2.3 Record information

Processing was performed using TSPP: Collection of FORTRAN programs for processing and manipulating time series, developed by Dr David Boore from the United States Geological Survey (Boore 2008). The ground-motion recordings were reformatted and converted into SMC-format files (see <http://nsmf.wr.usgs.gov/smcfmt.html> for details). When necessary, unevenly sampled data were interpolated and resampled at 200 samples per second. Before the application of any process-

ing procedure, non-standard noise (i.e., spurious spikes) encountered in digitized records from analogue instruments (Douglas 2003) was identified by visual inspection of the jerk (derivative of the acceleration trace). Spikes identified as erroneous, were removed by replacing the acceleration ordinate of the spike with the mean of the preceding and proceeding accelerations values. For some of the analogue recordings included in this database, instrument correction has been already applied by the data provider and thus was not applied here. Instrument corrections were not applied to the remaining records from analogue instruments in this database as, in some cases, complete information on the instruments response was not available and additionally, the application of an instrument correction can result in amplification of high-frequency noise introduced during the digitization process (Boore and Bommer 2005). As a result of the dynamic range of the digital instruments (natural frequencies of 100 Hz or higher) corrections for instrument characteristics were not applied to the digital recordings included in the database.

The records were processed in a consistent manner, with individual components individually filtered. Before performing the actual filtering of the record, an initial baseline correction was applied to the raw accelerogram (zeroth-order correction). The mean determined from the pre-event portion of the record or the mean computed from the whole record if the pre-event portion was not available was subtracted from the entire acceleration time series. After making this initial baseline correction, the acceleration traces were integrated without filtering, to check for long-period drifts that could indicate the presence of offsets in the reference baseline. In most cases, baseline offsets were small and the long-period noise was removed by filtering. The records were then filtered using an acausal bidirectional, eighth-order Butterworth filter. For digital records, low-cut filter frequencies were determined by considering the signal-to-noise ratio between each channel and a model of the noise obtained from the pre-event memory. Since this type of model does not account for “signal-generated” noise (Boore and Bommer 2005), the results were checked through visual inspection

of the velocity and displacement traces obtained from integration of the filtered acceleration record. Visual inspection of these traces was also the basis for the selection of the low-cut filter frequency when no pre-event memory of digital records was available. For analogue records, fixed traces were not available to allow the identification of low-frequency noise. Therefore, the Fourier Amplitude Spectrum (FAS) of the unfiltered accelerogram was compared with the noise spectrum estimated from studies of instruments and digitising apparatus such as those proposed by Lee and Trifunac (1990) and Skarlatoudis et al. (2003), which were used as guide for the selection of low-cut filters. Since these studies correspond to a particular combination of accelerograph and digitiser, which does not correspond to that of data being processed, visual examination of the velocity and displacement traces was also used as a basis for the selection of the low-cut filter frequency.

In selecting low-cut filter frequencies, the filter parameter was chosen to give a signal-to-noise ratio of 2. It is noted that the comparison of the FAS of the record with that of the noise indicates the ratio of signal-plus-noise to noise, hence if the desired target is a signal-to-noise ratio of 2, the ratio of the record FAS to that of the noise model should be 3. The maximum usable period of the spectrum was then defined as 0.8 times the low-cut filter period, as suggested by Abrahamson and Silva (1997), which is broadly consistent with the limits suggested by Akkar and Bommer (2006). On this basis, it was decided that for about 85% of the records included in the database, the spectral ordinates could be reliably calculated up to 3 s (or up to 4 s or longer for digital records), although for a few analogue accelerograms, the usable period range could only be extended up to 2 s. Finally, removal of high-frequency noise was achieved by using high frequency cut-off filters at 25 Hz for records from analogue instruments and 50 Hz for records from digital instruments. Peak values of acceleration and velocity and acceleration response spectra values for 5% of the critical damping were then obtained from the processed data.

The other relevant parameter for each record is the source-to-site distance. The source-to-site

distance was characterised in terms of the closest distance to the earthquake fault plane or rupture distance (R_{rup}). Fault plane dimensions and orientations were obtained from published finite-source rupture models when available (e.g., Abe 1972; Hartzell and Langer 1993; Mendoza et al. 1994; Choy and Dewey 1988; Pritchard et al. 2007; Ji and Zeng 2007). Events for which fault-plane geometries from finite-fault inversion were available have moment magnitudes $7.1 \leq M_W \leq 8.4$ and contribute 70% of the strong-motion data included in the database. For the 1966 (M_W 8.1) and 1970 (M_W 8.0) Peruvian earthquakes, the rupture areas assumed for source-to-site distance computations were those estimated by Abe (1972) based on early aftershocks distributions; these two events only contribute two records. For the aftershocks of the 1985 Valparaiso event, with moment magnitudes $6.3 \leq M_W \leq 7.1$, the circular rupture geometries determined by Choy and Dewey (1988) were used to estimate the corresponding rupture distances.

For the remaining events, for which neither finite-source models nor reliable distributions of early aftershocks were available, an alternative approach was used to estimate the distance metrics. Fault-rupture dimensions were estimated from empirical relationships between rupture area and moment magnitude (M_W) for interface and intraslab-type events that have been determined in Strasser et al. (2010). The rupture plane was then located in space, assuming that the epicentre lies above the centre of a dipping plane. The strike, dip and rake of the fault plane were assumed to correspond to the preferred focal plane of the two sets of angles listed in the Harvard CMT catalogue. On the other hand, for intraslab-type events the main focal plane was assumed to be that suggested by individual studies of these events. For instance, for the 15 October 1997 (M_W 7.1) Punitaqui event, the orientation of the actual fault plane was estimated to be the almost vertical nodal plane of the two sets of angles reported in the Harvard CMT catalogue, based on the body-wave modelling for this event carried out by Lemoine et al. (2001). Similarly, the orientation of the preferred focal planes for the 7 November 1981 (M_S 6.7) and the 5 January 1974 (M_S 6.7) events used herein were those suggested by

Astiz et al. (1988) and Langer and Spence (1995), respectively. This approach is expected to be a reasonable approximation for the purpose of source-to-site distance calculations in view of the fact that most of the events for which this assumption was applied correspond to intraslab events with magnitude $5.9 \leq M_S \leq 6.8$, which were recorded at large distances and thus their fault dimensions are not likely to be very large compared to the source-to-site distances.

3 Conclusions

A database of strong-motion recordings for the Peru–Chile region from 1966 to 2007 has been compiled, with particular emphasis on the quality of both the data and the metadata associated with the recordings. The development of reliable regional strong-motion databases for subduction events is of prime importance as they increase the confidence in the results of both regional and global ground-motion prediction studies for subduction regimes. While the database presented in this study is not sufficient for the derivation of a new predictive equation for ground motions from subduction-type events in the Peru–Chile region, it significantly expands the global database of strong-motion data and associated metadata that can be used in the derivation of predictive equations for subduction environments. Indeed, the compiled database further extends the magnitude range of the currently available global databases for interface events (e.g., Youngs et al. 1997; Atkinson and Boore 2003, 2008) by the inclusion of data from the 2001 (M_W 8.4) Peruvian event and further supplements the global intraslab data by the inclusion of recordings from the 2005 (M_W 7.8) Chilean event. Although the database presented in this paper includes strong-motion data recorded from 1966 to 2007, the present work can be easily extended to include more recordings and metadata from this region as they become available, including those from the M_W 8.8 earthquake that struck Chile on 27 February 2010, as this study was being finalised.

The compiled database will also allow the assessment of the existing predictive models for subduction-type events in terms of their suitability

for this region, which directly influences seismic hazard assessment in this region.

Acknowledgements The doctoral research of the first author, on which this paper is based, has been partially funded by the Alþan Programme of the European Union under scholarship E05D053967CO and the COLFUTURO programme; their financial support is gratefully acknowledged. The authors thank Bertrand Delouis for providing information on the source process of the 13 June 2005 Chilean earthquake.

We are grateful to two anonymous reviewers for their constructive feedback that helped to improve the manuscript.

References

- Abe K (1972) Mechanics and tectonic implications of the 1966 and 1970 Peru earthquakes. *Phys Earth Planet Inter* 5:367–379
- Abrahamson NA, Silva WJ (1997) Empirical response spectral attenuation relations for shallow crustal earthquakes. *Seismol Res Lett* 68(1):94–127
- Aguilar Bardales Z, Alva Hurtado J (2007) Seismic microzonation of Lima. In: Proceedings of the international conference on earthquake engineering, Centro Peruano Japonés de Investigaciones Sísmicas y Mitigación de Desastres (CISMID), Universidad Nacional de Ingeniería, Lima, Peru. Available online at: http://www.cismid.edu.uni.pe/descargas/redacis/redacis32_p.pdf. Last accessed November 2009 (in Spanish)
- Akkar S, Bommer JJ (2006) Influence of long-period filter cut-off on elastic spectral displacements. *Earthq Eng Struct Dyn* 35(9):1145–1165
- Alva Hurtado J (2005) Sismo de Intraplaca ocurrido en Tarapacá el 13 de Junio del 2005. Presentation at the Centro Peruano Japonés de Investigaciones Sísmicas y Mitigación de Desastres (CISMID), Universidad Nacional de Ingeniería, Lima, Peru (in Spanish)
- Araneda C, Saragoni GR (1994) Project of geological survey of strong motion site in Central Chile. Report for the Kajima Institute of Construction Technology of Tokyo, Santiago, Chile
- Astiz L, Lay T, Kanamori H (1988) Large intermediate-depth earthquakes and the subduction process. *Phys Earth Planet Inter* 53(1–2):80–166
- Atkinson GM, Boore DM (2003) Empirical ground-motion relations for subduction-zone earthquakes and their application to Cascadia and other regions. *Bull Seismol Soc Am* 93(4):1703–1729
- Atkinson GM, Boore DM (2008) Erratum to: Empirical ground-motion relations for subduction-zone earthquakes and their application to Cascadia and other regions. *Bull Seismol Soc Am* 98(4):2567–2569
- Barazangi M, Isacks BL (1976) Spatial distribution of earthquakes and subduction of the Nazca plate beneath South America. *Geology* 4(11):686–692
- Beck S, Barrientos S, Kausel E, Reyes M (1998) Source characteristics of historic earthquakes along the central Chile subduction zone. *J South Am Earth Sci* 11(2):115–129
- Bernal I, Tavera H (2007a) Peak accelerations recorded in the City of Lima. In: The August 15, 2007 (7.0 ML) Pisco Earthquake (Preliminary report). Dirección de Sismología, Instituto Geofísico del Perú (IGP) (in Spanish)
- Bernal I, Tavera H (2007b) Peak accelerations recorded in the City of Ica. In: The August 15, 2007 (7.0 ML) Pisco Earthquake (Preliminary report). Dirección de Sismología, Instituto Geofísico del Perú (IGP) (in Spanish)
- Boore DM (2008) TSPP: a collection of FORTRAN programs for processing and manipulating time series. Available online from http://www.daveboore.com/software_online.htm. Last accessed December 2009
- Boore DM, Bommer JJ (2005) Processing of strong-motion accelerograms: needs, options and consequences. *Soil Dyn Earthqu Eng* 25(2):93–115
- Boroschek R, Comte D (2006) Amplitude and frequency characteristics of the 2001 Southern Peru, $M_w = 8.4$ earthquake records. *J Seismol* 10(3):353–369
- Cahill T, Isacks BL (1992) Seismicity and shape of the subducted Nazca plate. *J Geophys Res* 97(B12):17503–17529
- Campbell KW, Algermissen ST, Kausel E, Highland LM (1989) Processed strong-motion data for the Central Chile earthquake of March 3, 1985: fifteen accelerometer sites owned by CHILECTRA, ENDESA, and the Department of Geology and Geophysics, University of Chile. Open-File Report 89–448, US Geological Survey, 328 pp
- Campbell KW, Algermissen ST, Kausel E, Highland LM (1990) Processed strong-motion data for the Central Chile aftershock of April 9, 1985: nine accelerometer sites owned by CHILECTRA, ENDESA, and the Department of Geology and Geophysics, University of Chile. Open-File Report 90–46, US Geological Survey, 171 pp
- Çelebi M (1987) Topographical and geological amplifications determined from strong-motion and aftershock records of the 3 March 1985 Chile earthquake. *Bull Seismol Soc Am* 77(4):1147–1167
- Çelebi M (1988) Processed Chile earthquake records of 3 March 1985 and aftershocks. Open-File report 87–195, revised October 1988, US Geological Survey, 254 pp
- Choy GL, Dewey JW (1988) Rupture process of an extended earthquake sequence: teleseismic analysis of the Chilean earthquake of March 3, 1985. *J Geophys Res* 93(B2):1103–1118
- Cifuentes IL (1989) The 1960 Chilean earthquakes. *J Geophys Res* 94(B1):665–680
- Comte D, Pardo M (1991) Reappraisal of great historical earthquakes in the northern Chile and southern Peru seismic gaps. *Nat Hazards* 4(1):23–44
- Comte D, Suárez G (1995) Stress distribution and geometry of the subducting Nazca plate in northern Chile

- using teleseismically recorded earthquakes. *Geophys J Int* 122(2):419–440
- Comte D, Eisenberg A, Lorca E, Pardo M, Ponce I, Saragoni R, Singh SK, Suárez G (1986) The 1985 Central Chile earthquake: a repeat of previous great earthquakes in the region? *Science* 233(4762):449–453
- Comte D, Pardo M, Dorbath L, Dorbath C, Haessler H, Rivera L, Cisternas A, Ponce L (1994) Determination of seismogenic interplate contact zone and crustal seismicity around Antofagasta, northern Chile using local data. *Geophys J Int* 116(3):553–561
- Cortez-Flores A (2004) Site response of the 2001 Southern Peru earthquake. MSc Thesis, Washington State University
- Delouis B, Legrand D (2007) M_w 7.8 Tarapaca intermediate depth earthquake of 13 June 2005 (northern Chile): fault plane identification and slip distribution by waveform inversion. *Geophys Res Lett* 34(1):Article No. L01304
- Delouis B, Cisternas A, Dorbath L, Rivera L, Kausel E (1996) The Andean subduction zone between 22 and 25°S (northern Chile): precise geometry and state of stress. *Tectonophysics* 259(1–3):81–100
- DeMets C, Gordon RG, Argus DF, Stein S (1990) Current plate motions. *Geophys J Int* 101(2):425–478
- Dorbath L, Cisternas A, Dorbath C (1990) Assessment of the size of large and great historical earthquakes in Peru. *Bull Seismol Soc Am* 80(3):551–576
- Douglas J (2003) What is a poor quality strong-motion record? *Bull Earthquake Eng* 1(1):141–156
- EERI (1986) The Chile earthquake of March 3, 1985—EERI reconnaissance report. *Earthq Spectra* 2(2):249–508
- EERI (2007) Learning from earthquakes: the Pisco, Peru, earthquake of August 15, 2007. EERI Special Earthquake Report, EERI Newsletter, October 2007
- Engdahl ER, Villaseñor A (2002) Global seismicity: 1900–1999. In: Lee WHK, Kanamori H, Jennings PC, Kisslinger C (eds) *International handbook of earthquake and engineering seismology*. Academic, New York, pp 665–690
- Engdahl ER, van der Hilst R, Buland R (1998) Global teleseismic earthquake relocation with improved travel times and procedures for depth determination. *Bull Seismol Soc Am* 88(3):722–743
- Espinosa AF, Husid R, Algermissen ST, De las Casas J (1977) The Lima earthquake of October 3, 1974; intensity distribution. *Bull Seismol Soc Am* 67(5):1429–1439
- Hartzell S, Langer C (1993) Importance of model parameterization in finite fault inversions: application to the 1974 M_w 8.0 Peru earthquake. *J Geophys Res* 98(B12):22123–22134
- International Seismological Centre (2009) EHB Bulletin. <http://www.isc.ac.uk/search/bulletin/ehb.html>. Last accessed May 2009
- Ji C, Zeng Y (2007) Preliminary results of the August 15, 2007 M_w 8.0 coast of central Peru earthquake. US Geological Survey web report. Available online at http://earthquake.usgs.gov/eqcenter/eqinthenews/2007/us2007gbcv/finite_fault.php. Last accessed November 2009
- Jordan TE, Isacks BL, Allmendinger RW, Brewer JA, Ramos VA, Ando CJ (1983) Andean tectonics related to geometry of subducted Nazca plate. *Bull Geol Soc Am* 94(3):341–361
- Kausel E (1986) Los Terremotos de Agosto de 1868 y Mayo de 1877 que afectaron el Sur del Peru y Norte de Chile. *Bol Acad Chil Cienc* 3:8–12
- Kelleher JA (1972) Rupture zones of large South American earthquakes and some predictions. *J Geophys Res* 77(11):2087–2103
- Langer CJ, Spence W (1995) The 1974 Peru earthquake series. *Bull Seismol Soc Am* 85(3):665–687
- Lee VW, Trifunac MD (1990) Automatic digitization and processing of accelerograms using PC. Report CE-90-03, Department of Civil Engineering, University of Southern California, Los Angeles, California, 115 pp
- Lemoine A, Madariaga R, Campos J (2001) Evidence for earthquake interaction in Central Chile: the July 1997–September 1998 sequence. *Geophys Res Lett* 28(14):2743–2746
- Lemoine A, Madariaga R, Campos J (2002) Slab-pull and slab-push earthquakes in the Mexican, Chilean and Peruvian subduction zones. *Phys Earth Planet Inter* 132(1–3):157–175
- Lomnitz C (2004) Major earthquakes of Chile: a historical survey, 1535–1960. *Seismol Res Lett* 75(3):368–378
- Luppichini N (2004) Interpretación de los acelerogramas del terremoto de Chile Central de 1985 considerando ondas sísmicas de alta frecuencia. Civil Engineering Dissertation, University of Chile
- McVerry G, Zhao J, Abrahamson N, Somerville P (2006) New Zealand acceleration response spectrum attenuation relations for crustal and subduction zone earthquakes. *Bull N Z Soc Earthq Eng* 39(1):1–58
- Mendoza C, Hartzell S, Monfret T (1994) Wide-band analysis of the 3 March 1985 central Chile earthquake: overall source process and rupture history. *Bull Seismol Soc Am* 84(2):269–283
- Midorikawa S (1992) Site effects on strong-motion records of the 1985 Chile earthquake and their non-linear behaviour. In: *Proceedings of the 10th World Conference in Earthquake Engineering*, vol 2, Madrid, Spain, 19–24 July, pp 1031–1036
- Midorikawa S, Riddell R, Cruz E (1991) Strong-motion accelerograph array in Santiago, Chile, and preliminary evaluation of site effects. *Earthq Eng Struct Dyn* 20(5):403–407
- NEHRP (1997) Recommended provisions for seismic regulations for new buildings and other structures. Report FEMA 303, US Federal Emergency Management Agency, Washington, DC
- Nishenko SP (1985) Seismic potential for large and great interplate earthquakes along the Chilean and southern Peruvian margins of South America: a quantitative reappraisal. *J Geophys Res* 90(B5):3589–3616
- Pacheco JF, Sykes LR (2002) Seismic moment catalog of large shallow earthquakes, 1900 to 1989. *Bull Seismol Soc Am* 82(3):1306–1349

- Pardo M, Comte D, Monfret T, Boroschek R, Astroza M (2002a) The October 15, 1997 Punitaqui earthquake ($M_w=7.1$): a destructive event within the subducting Nazca plate in central Chile. *Tectonophysics* 345(1–4):199–210
- Pardo M, Comte D, Monfret T (2002b) Seismotectonic and stress distribution in the central Chile subduction zone. *J South Am Earth Sci* 15(1):11–22
- Pritchard M, Norabuena E, Ji C, Boroschek R, Comte D, Simons M, Dixon T, Rosen P (2007) Geodetic, teleseismic, and strong motion constraints on slip from recent southern Peru subduction zone earthquakes. *J Geophys Res* 112(B3):1–24
- Riddell R (1995) Inelastic design spectra accounting for soil conditions. *Earthq Eng Struct Dyn* 24(11):1491–1510
- Rodriguez-Marek A, Bray JD, Abrahamson N (2001) An empirical geotechnical seismic site response procedure. *Earthq Spectra* 19(3):653–675
- Rodriguez-Marek A, Hurtado J, Cox B, Meneses J, Moreno V, Olcese M, Sancio R, Wartman J (2007) Preliminary reconnaissance report on the geotechnical engineering aspects of the August 15, 2007 Pisco, Peru Earthquake. Report of the National Science Foundation-Sponsored Geotechnical Earthquake Engineering Reconnaissance (GEER) Team. Web report available from: http://gees.usc.edu/GEER/Peru_2007/Peru_2007_WebPage/index.htm. Last accessed November 2009
- Rosenblad BL, Bay JA (2008) Shear wave velocity profiles determined from SASW measurements at sites affected by the August 15th, 2007 earthquake in Peru. Report prepared for CERESIS, January 2008, 60 pp
- Ruiz S, Saragoni G (2005) Attenuation equations for subduction-zone earthquakes in Chile considering two seismogenic mechanisms and site effects. Proceedings, IX Jornadas Chilenas de Sismología e Ingeniería Antisísmica, Concepción, Chile, 16–19 November 2005. Paper No. A01–15 (in Spanish)
- Skarlatoudis A, Papazachos C, Margaris B (2003) Determination of noise spectra from strong motion data recorded in Greece. *J Seismol* 7(4):533–540
- SNGM (1982) 1:250,000 geologic map of Chile. Servicio Nacional de Geología y Minería, Chile
- Stauder W (1975) Subduction of the Nazca plate under Peru as evidenced by focal mechanisms and by seismicity. *J Geophys Res* 80(8):1053–1064
- Strasser FO, Arango MC, Bommer JJ (2010) Scaling of source dimensions for interface and intraslab subduction-zone earthquakes with moment magnitude. *Seismol Res Lett* (in press)
- Suárez G, Comte D (1993) Comment on ‘Seismic coupling along the Chilean subduction zone’ by BW Tichelaar and LR Ruff. *J Geophys Res* 98(B9):15825–15828
- Tavera H, Bernal I (2005) Spatial distribution of rupture areas and seismic gaps in western Peru. Special volume N6 commemorating Alberto Giesecke, Geological Society of Peru, pp 89–92 (in Spanish)
- Tavera H, Bernal I, Strasser FO, Arango-Gaviria MC, Alarcon JE, Bommer JJ (2008) Ground motions observed during the 15 August 2007 Pisco, Peru, earthquake. *Bull Earthq Eng* 7(1):71–111
- Tavera H, Buforn E, Bernal I, Antayhua Y, Vilacapoma L (2002) The Arequipa (Peru) earthquake of June 23, 2001. *J Seismol* 6(2):279–283
- Tichelaar BW, Ruff LJ (1991) Seismic coupling along the Chilean subduction zone. *J Geophys Res* 96(B7):11997–12022
- Wells DL, Coppersmith KJ (1994) New empirical relationships among magnitude, rupture length, rupture width, rupture area, and surface displacement. *Bull Seismol Soc Am* 84(4):974–1002
- Youngs RR, Chiou SJ, Silva WJ, Humphrey JR (1997) Strong ground motion attenuation relationships for subduction zone earthquakes. *Seismol Res Lett* 68(1):58–77
- Zhao J, Irikura K, Zhang J, Fukushima Y, Somerville P, Asano A, Ohno Y, Oouchi T, Takahashi T, Ogawa H (2006a) An empirical site-classification method for strong-motion stations in Japan using H/V response spectral ratio. *Bull Seismol Soc Am* 96(3):914–925
- Zhao JX, Zhang J, Asano A, Ohno Y, Oouchi T, Takahashi T, Ogawa H, Irikura K, Thio HK, Somerville PG, Fukushima Y (2006b) Attenuation relations of strong ground motion in Japan using site classification based on predominant period. *Bull Seismol Soc Am* 96(3):898–913